PHYSICAL REVIEW B **74**, 214204 (2006)

Short- and medium-range structure of amorphous zircon from molecular dynamics simulations

Jincheng Du,[1,*] Ram Devanathan,[1] L. René Corrales,[1,†] William J. Weber,[1] and Alastair N. Cormack[2]
[1]*Fundamental Science Directorate, Pacific Northwest National Laboratory, Richland, Washington 99352, USA*
[2]*School of Engineering, Alfred University, Alfred, New York 14802, USA*

(Received 15 March 2006; revised manuscript received 11 July 2006; published 18 December 2006)

We have simulated the structure of amorphous zircon using classical molecular dynamics simulations with a partial-charge model. We present detailed structural characterizations of the simulated high and low density amorphous zircon, and compare our results with available neutron diffraction, EXAFS, NMR and other experimental results. The results show that amorphization leads to polymerization of the silicon-oxygen network and the formation of regions rich in zirconium. The average n value of Q^n species is 1.6–1.8, where a considerable percentage of the oxygen ions (around 20%) have only zirconium in the first coordination shell in amorphous zircon. The Zr-O bond length (around 2.10 Å) is shorter and the oxygen coordination number around zirconium smaller (6–7) than in crystalline zircon, in good agreement with the EXAFS results. The calculated static neutron structure factors show reasonable agreement with experimental result. The medium range structures were characterized by the first sharp diffraction peak and primitive ring analysis, as well as from Q_n distribution, oxygen environment and cation-cation pair distribution. It is found that most of the silicon-oxygen tetrahedra form branched chains and rings of various sizes, while the zircon-oxygen polyhedra form a percolated network different from the crystalline percolated structure.

DOI: 10.1103/PhysRevB.74.214204 PACS number(s): 61.43.−j, 68.03.Hj, 61.43.Bn, 31.15.Qg

INTRODUCTION

Amorphous zircon has drawn considerable attention in recent years due to both scientific and technological interests. Zircon has been used in geochronology studies and is a natural candidate for the immobilization of excess plutonium and transuranic waste due to its chemical and physical durability.[1,2] Natural zircon becomes amorphous over hundreds of millions of years from the accumulation of radiation damage from the alpha decay of its radioactive actinide constituents, where the amorphous form of natural zircon is often referred to as the metamict state.[1,3] Amorphization dramatically changes the zircon structure, chemical durability and physical properties that are vital to applications such as geochronology and nuclear waste forms.[2,4,5] Amorphous zircon also has applications in optical waveguides[6] and as a thin-film optical coating.[7] Recently, there has been active research interest in zircon-based thin-film high-K dielectric materials in complementary metal oxide semiconductors (CMOS) to replace current silica glass films.[3,8,9] The amorphous zircon structure is stable in direct contact with silicon and has a higher dielectric constant that results in lower leaking current in sub 100 nm line width CMOS devices.[8]

The amorphous form of zircon can not be obtained from normal melting and quenching routes because the zircon melt phase separates and quenches into crystalline zirconia and silica glass.[10] However, radiation damage accumulation and ion implantation can amorphize crystalline zircon and the amorphous form obtained by both of these approaches are found to have similar structure.[1] Significant volume swelling is found to accompany the amorphization process. In the fully amorphized form, the volume swelling is 16.6% in Pu-doped zircon and 18.4% in natural zircon relative to the original crystalline state.[1] Amorphous zircon can also be formed using reactive magnetron sputtering[7] and sol-gel processing,[11] where a volume expansion of 17.7% relative to the crystalline state was observed.[11] The amorphous zircon obtained by different methods appears to have similar volume expansion relative to the crystalline form.

Understanding the atomic structure of amorphous zircon is crucial to the study of the amorphization and annealing processes of zircon, chemical stability of zircon as a nuclear waste form, and the dielectric properties of zircon thin films.[3,12] Due to the complex structure and lack of long range order in amorphous materials, there is relatively limited knowledge of atomic structure of the amorphous zircon. The purpose of this work is to study the amorphous zircon structure using a new set of effective potential models. The partial-charge model used here is capable of correctly describing the structural and mechanical properties of the zircon, zirconia, and silica crystal and amorphous phases. Through carefully designed simulations, insights into the structure modifications that lead to increased leaching and dissolution rate of amorphous zircon relative to the crystalline form are gained through structure analyses including the extent of polymerization of the silicon-oxygen network, the change of coordination environment and clustering behavior of zirconium ions in amorphous zircon.

There have been considerable experimental efforts in the study of the amorphous zircon structure. Extended x-ray absorption fine structure (EXAFS) is a very sensitive way to probe the local environments of cations in glass and amorphous materials. Detailed EXAFS studies of natural metamict zircons have found that the Zr-O distance decreases by 0.06 Å and the zirconium coordination number decreases from 8 in crystalline zircon to 7 in the metamict form.[13] A decrease of Zr-Zr distance by 0.3 Å was also observed in metamict zircon.[13] In a subsequent study of the annealing of metamict zircon, it was found that the average oxygen coordination number around Zr in metamict zircon ranges from 6.8 to 7.2.[14] Based on EXAFS and x-ray diffraction (XRD) results, it has been suggested that there exist nano-sized Zr- and Si-rich domains in metamict zircons that are several hun-

©2006 The American Physical Society

dred million years old.[14] The amorphous structure created in just over a decade in ^{238}Pu-doped zircon was studied using XRD and EXAFS,[15] where it was found that, although the material lacked long-range order, the distorted zircon structure was retained over a length scale of 0.5 nm; however, the above-mentioned shortening of Zr-O bond length and decrease of oxygen coordination number of zirconium found in natural metamict zircons were not observed.[15] Solid state nuclear magnetic resonance (NMR) of ^{29}Si is sensitive to the change of polymerization in silicate materials and has been used to study the change of SiO_4 Q^n species, meaning n bridging oxygens per tetrahedron, in zircon exposed to different levels of radiation damage.[16,17] A sharp peak centered at about −81.6 ppm was observed in crystalline zircon minerals and was assigned to isolated SiO_4 tetrahedra (Q^0).[18] As the accumulated alpha-decay dose increases, the peak broadens and gradually moves to higher chemical shifts.[16] The broad peak of fully amorphized zircon corresponds to a combination of Q^n species with n ranging from 0 to 4. The average n value was estimated to range from 2 to 3; this value is high compared to the oxygen ions gained from the decrease of zirconium coordination number, which led the authors to suggest the existence of interstitial oxygens.[16] Later *ab initio* MD simulation[19] of amorphous zircon and subsequent calculation of the NMR spectra has shown that the average n value of Q_n species from the above mentioned NMR study was overestimated due to the use of improper empirical scale to interpret the NMR data, and an average n of 1.5 can account for the experimental spectra.[16] The only available neutron diffraction study of amorphous zircon with ^{238}Pu doping shows a diffraction spectra that confirms full amorphization of the sample and no phase separation in this relatively young material,[20] and the pair distribution function suggests that the structural units in zircon were largely preserved.[20] Infrared (IR) and Raman spectroscopy have also been used to characterize the amorphous structure of natural metamict zircons.[21–24] Early IR spectroscopy studies proposed the decomposition of zircon into end member oxides as a result of metamictization[21] but this is not supported by more recent IR and Raman work.[22–24] Raman spectra of natural zircons exhibiting different levels of radiation damage show that peaks corresponding to SiO_4 tetrahedra stretching and bending soften with increasing radiation damage.[24] Compared to the Raman spectra of silica, the SiO_4 tetrahedra were found to be less polymerized in metamict zircon.[24] The slight differences in amorphous structure observed between the relatively young Pu-doped zircon and the aged natural metamict zircons may suggest that some local relaxation may be occurring over hundreds of millions of years in the natural zircons, which is not yet evident in the decades old Pu-doped zircon.

Molecular dynamics (MD) simulations employing both empirical potentials[25] and first principle methods[19] have been used to study the amorphous structure of zircon. These simulations provided detailed atomic structure information on amorphous zircon. In the *ab initio* MD simulations of zircon,[19] polymerization of the silicon-oxygen units, segregation of zirconium atoms and the decrease of zirconium coordination number were observed. An average polymerization of $Q^{1.5}$ was found in the low density amorphous zircon.[19] This value is consistent with the experimental findings of Farnan and Saije,[16] when a correction is applied to the empirical scale used to interpret the NMR data.[19]

A recent study used a different partial-charge Born-Mayer type potentials to simulate amorphous zircon with two densities.[25] Polymerization of Si-O network was observed with average n value of 2 for the Q^n distribution in the low density phase. The coordination number of zirconium was found to decrease to around 7 in the low density phase. However, the simulated high density amorphous zircon structure seemed to be more like a distorted zircon crystalline lattice since both coordination of silicon and zirconium are largely unchanged and the polymerization and change of bond angle distribution compared to the crystal is very low. The coordination number of silicon had an average value of 3.5 in the low density amorphous phase, lower than the normal tetrahedral coordination of silicon in silicate materials. This appears to be related to the different cation charges of zirconium (+3.8) and silicon (+2.0).[25] Although this set of partial-charge potential gives excellent description of the structure and mechanical properties of crystal zircon, the disparity of the zircon and silicon charges can cause local charge neutrality problem in highly defected crystalline regions and within the amorphous structure. The potential model used in this work has the strengths in that it is transferable between end member oxides and zircon and can be used effectively in large scale simulations. This makes it desirable to overcome some of the shortcomings of the previous simulations to obtain insight into the amorphous structure of zircon.

This paper is arranged in the following way. The next section describes the potential models and procedures used to simulate the melting of zircon and the generation of the amorphous zircon structures. This is followed by the results section that describes the comparison of structure and properties of crystalline zircon using several previously proposed potential models and the one used in this work, the melting processes for zircon, and characterization of amorphous zircon structures. Comparison with experimental data including neutron diffraction, EXAFS and NMR are also presented. A discussion is then presented on the polymerization and clustering in the amorphous structures, the effects of simulation cell size and density of the amorphous structure. The results of this work are summarized in the conclusion.

SIMULATION DETAILS

Potential models play a critical role in the classical molecular dynamics simulations. The study of collision cascade in zircon using molecular dynamics demands efficient and effective potential models. Since highly defected and amorphous regions are produced in collision cascades, the potential models used must be able to not only describe the equilibrium crystal structure and properties of zircon, but also the native defects and amorphous zircon structures. Because phase decomposition and recrystallization of amorphous zircon into silica and zirconia has been observed experimentally under some conditions,[10,14] the potential model should also be able to simulate these oxides. The Teter potential model introduced in this work satisfies these requirements

TABLE I. Atomic charges and Buckingham potential parameters.

Pairs	A (eV)	ρ (Å)	C (eV Å^6)
$Si^{2.4}$-$O^{-1.2}$	13702.905	0.193817	54.681
$O^{-1.2}$-$O^{-1.2}$	2029.2204	0.343645	192.58
$Zr^{2.4}$-$O^{-1.2}$	7747.1834	0.252623	93.109

and is desirable for the study of amorphous structure of zircon.

The potentials used in this study are partial-charge pair potentials with the parameters developed by D. M. Teter.[26] The atomic charges on silicon and zircon ions are both +2.4 and charge of oxygen ion is −1.2. This leads to charge neutrality in the zircon structure as well as for the pure states of zirconia and silica. Short range interactions have the Buckingham form that contains an exponential repulsive term and a power dispersion term to describe the van der Waals interactions. The interatomic potential between atom i and j has the form

$$V(r_{ij}) = \frac{q_i q_j e^2}{4\pi\varepsilon r_{ij}} + A\exp(-r_{ij}/\rho) - C/r_{ij}^6, \qquad (1)$$

where q_i and q_j are the atomic charges, r_{ij} is the distance between atom i and j, A, ρ, and C are Buckingham parameters. The atomic charges and potential parameters are listed in Table I. Due to the dominance of the power term at short interatomic distances, the total Buckingham potential energy goes to negative infinity when r approaches zero that leads to unphysical fusion of atoms. This problem was corrected by splicing the Ziegler-Biersack-Littmark (ZBL)[27] potential, which provides a realistic repulsive force at short interatomic distances. The ZBL potential is essentially a screened Coulombic repulsion potential that has the form,

$$V^{ZBL}(r_{ij}) = \frac{z_i z_j e^2}{4\pi\varepsilon r_{ij}} \cdot \sum_{k=1}^{4} a_k \exp\left(-\frac{r_{ij}\cdot b_k}{a_o}\right), \qquad (2)$$

where z_i and z_j are the core charges, a_k and b_k are universal parameters, and a_o is the Bohr radius. The Buckingham (together with the Coulombic interactions) and the ZBL potentials were smoothly connected using a splice function. The splice function is a combination of power and exponential terms with the parameters determined by ensuring the potential, force and the first derivative of the force are continuous at the splice points. The final total potential is smooth and monotonic.

Molecular dynamics simulations were performed using DL_POLY, a program developed by Smith and Forester in Daresbury Laboratory, UK.[28] Coulombic interactions were evaluated using the Ewald summation method with a relative precision of 10^{-6}. The short-range interaction cutoff was 8.0 Å. Integration of the equations of motion was performed using the Verlet Leapfrog algorithm with a time step of 10^{-15} second. The Berendsen thermostat was used in constant volume and constant temperature (NVT) ensemble MD simulations, and the Nosé-Hoover thermostat and barostat were used in constant pressure and constant temperature (NpT) ensemble MD simulations.

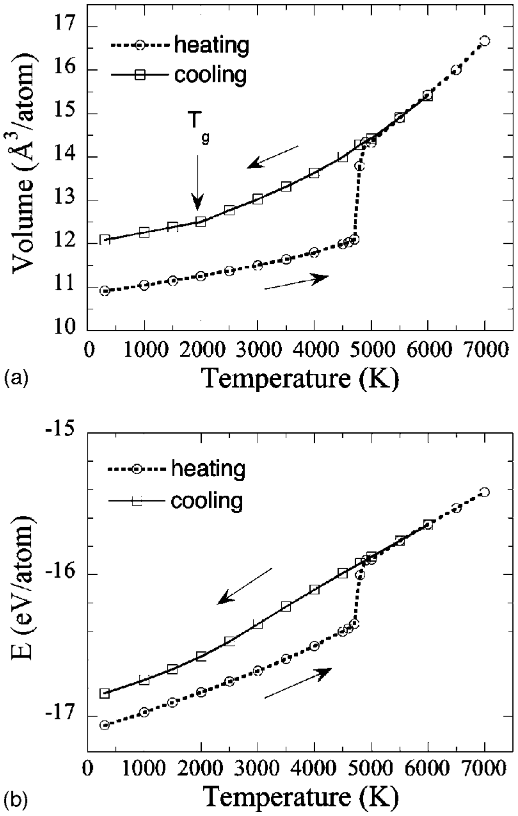

FIG. 1. Volume (a) and potential energy (b) versus temperature during heating and cooling of zircon at constant pressure.

Three zircon super cells of 4×4×4, 6×6×6, and 8×8×8 unit cells based on the experimental zircon crystal structure were built with total atom numbers of 1536, 5184, and 12288, respectively. The melting of zircon was studied with the 4×4×4 and 6×6×6 super cells using the NpT ensemble with zero applied pressure. The system temperature was increased gradually from 300 K to 7000 K for 100,000 simulation steps (100 ps) at each temperature. As shown in Fig. 1, the zircon crystal shows a well-defined melting point at around 4800 K. Subsequent cooling leads to an amorphous zircon phase with around 11 percent volume expansion with respect to the zircon crystal. This amorphous phase represents the optimal amorphous density for this model potential and will be named high density (HD) amorphous zircon in comparison to the low density (LD) form that is constrained to the experimental volume of 18 percent volume swelling. The melting process studied using both 4×4×4 and 6×6×6 super cells gave essentially identical results suggesting little size effect in the simulated melting.

An amorphous zircon sample with experimentally observed 18% volume swelling relative to the zircon crystal was simulated at constant volume (NVT). This lower density amorphous zircon is named LD. (The name and size of simulated zircon structures are summarized in Table II.) The simulation cell of the zircon melt at 6000 K obtained from gradually increasing the temperature of the starting crystal-

TABLE II. Simulated crystalline and amorphous zircon ($ZrSiO_4$).

Name	Unit cell expansion	Total number of atoms	Cell a/c parameters (Å)	Volume relative to crystal
Crystal	4×4×4	1536	26.2/24.3	1.0
HD	4×4×4	1536	27.1/25.2	1.11
LD	4×4×4	1536	27.6/25.7	1.18
LD-big	8×8×8	12288	55.3/51.3	1.18

line phase (4×4×4 super cell) using the NpT ensemble was resized to a volume corresponding to 18% swelling of the fully amorphous zircon. The melt was sequentially cooled to 6000, 5500, 5000, 4500, and 4000 K, with a 200 ps (200,000 steps) in the NVT ensemble followed by a 200 ps run in the constant volume and constant energy (NVE) ensemble at each temperature to allow full equilibration at each temperature. Below 4000 K, the system was cooled gradually to 300 K by continuously scaling the temperature every 250 steps for 370 ps, corresponding to a cooling rate of 2.4 K/ps. At 300 K, the glass was further equilibrated for 200 ps NVT and 200 ps NVE MD simulations. The final structure data of all the glasses were collected every 50 steps during the final 20,000 steps in the NVE runs. To study the simulation cell size effect on the amorphous zircon structure, two lower density amorphous zircon structures were simulated using the above procedure: one started from 4×4×4 zircon super cell with 1536 atoms (named LD) and the other started from 8 ×8×8 super cell with 12288 atoms (named LD-big).

The evolution of the temperature, pressure, total energy, as well as structure information such as cation coordination number and Q_n species, were monitored during the simulation processes. The reported final structure of each of the amorphous zircon phases were obtained by averaging over 400 configurations with each separated by 50 time steps at the end of the simulations with the NVE ensemble at 300 K. For comparison with the amorphous phases, crystalline zircon with a 4×4×4 super cell was also simulated at 300 K. A 200 ps run under NVT ensemble was followed by 200 ps runs in the NVE ensemble. The structure analyses of crystal zircon were performed in the same way as for the amorphous phases described above.

RESULTS

The tetragonal zircon structure has a space group of $I4_1/amd$ (No. 141) with 4 formula units of $ZrSiO_4$ (24 atoms) per unit cell.[29] Each unit cell can be further divided into two primitive cells with each containing two formula units. The Zr and Si atoms take the 4*a* and 4*b* Wyckoff sites at (0,3/4,1/8) and (0,1/4,3/8), respectively. The O atoms take the 16*h* Wyckoff sites at $(0,u,v)$ with u and v being internal parameters. The zircon structure is comprised of edge sharing ZrO_8 dodecahedra and SiO_4 tetrahedra forming chains along the [001] direction. These chains are cross-linked by further edge-sharing of ZrO_8 dodecahedra between chains. Four Zr-O bonds that share edges with SiO_4 are slightly longer than the other four Zr-O bonds that share corners with SiO_4 in each ZrO_8. Each oxygen atom bonds to two zircon and one silicon atom. The SiO_4 tetrahedra are slightly enlongated along the [001] direction leading to two O-Si-O bond angles of approximately 97 degrees and 116 degrees.

Table III compares the calculated zircon structure using Teter and three other potential models from the literature along with those from experiments.[29,30] All four sets of potentials give satisfactory description of the structure of zircon. The Teter potential used in this work consists of partial-charge pair wise interactions with the form of Buckingham. The partial atomic charges in the Teter potential are 2.4, 2.4, and −1.2 for Si, Zr, and O, respectively. An alternative partial-charge potential (referred to as the CEA potential) uses the charges of 2.0, 3.8, and −1.45 for Si, Zr, and O, respectively;[25] these potentials were used in a previous study of disordered zircon.[25] Both the Teter and CEA potentials reasonably reproduced the mechanical properties of zircon. The CDG[31,32] and PCW[33] potentials are full charge model potentials with the charge of zircon and silicon being 4.0, and the charge of oxygen being −2.0. The short range interactions in the PCW model also have the Buckingham form, and those in the CDG model has the Born-Mayer-Huggins form. Although the full charge models can simulate the crystal structure fairly well, their descriptions of the mechanical properties are less satisfactory. The CDG potential have the bulk modulus too low while the PCW too high. Another problem of the CDG potentials is that the difference between the two O-Si-O bond angles is too small, 12 degrees compared to 19 degrees in the experimentally measured structure. This can be attributed to the strong repulsion between oxygen such that the potential favors symmetric oxygen coordination around the silicon ions. The CEA partial-charge potential give the best fit to the structure and properties of crystalline zircon, which makes it excellent for the study of perfect crystals and point defects in zircon; however, the further away the local structure is modified from perfect zircon stoichiometry, the less well this potential will perform.[25] The Teter potential gives satisfactory description of both the structure and mechanical properties of zircon while providing identical partial charges for both zircon and silicon that maintains charge neutrality in isolated ZrO_2 and SiO_2 phases. In addition, this new set of potentials also gives a reasonable description of the structure and properties of the crystalline ZrO_2 and SiO_2 phases. Tables IV and V show the calculated structure parameters, bond length and bond angles, as well as properties, such as bulk modulus of alpha quartz and tetragonal zirconia model and the corresponding experimental data. The results indicate that both the ZrO_2

TABLE III. Comparison of the structure and properties of zircon of this work, the results obtained using three other empirical potential models and those from experiments.

	Calculations				
	This work	CEA[a]	CDG[b]	PCW[c]	Experiments[d]
Lattice constants (Å)					
a	6.54	6.60		6.31	6.60
c	6.08	6.09		6.42	5.98
Unit cell volume (Å^3)	260.0	265.6	254	260.8	260.8
Internal parameter					
u	0.0653	0.0657		0.0652	0.0660
v	0.2070	0.1990		0.2005	0.1951
Bond distances (Å)					
Si-O	1.58	1.62	1.59	1.63	1.62
Zr-O	2.12	2.13	2.16	2.06	2.13
	2.35	2.32	2.36	2.42	2.27
Bond angles (°)					
O-Si-O	100	97	101	97	97
	115	116	113	119	116
Bulk modulus (GPa)	245	223	167	259	225
Elastic constants (GPa)					
C_{11}	497	445		505	424
C_{33}	475	479		522	490
C_{44}	110	84		119	114
C_{66}	56	64		0	49
C_{12}	104	64		72	70
C_{13}	149	123		172	150

[a] Reference 25.
[b] References 30 and 35.
[c] Reference 27.
[d] References 40 and 41.

and SiO_2 phases can be simulated with the current potential model. This makes the new potential ideal for the study of amorphous zircon and of more complex phenomena such as radiation induced amorphization and phase decomposition.

Figure 1 shows the melting process of crystalline zircon simulated under constant pressure and temperature ensemble (NpT). Both the volume [Fig. 1(a)] and the potential energy [Fig. 1(b)] versus temperature curves show a well-defined melting temperature near 4800 K. This high melting temperature is partly due to superheating that is usual in the simulation of defect-free crystal. There is a 19.5% volume increase and a 3.1% (0.44 eV/atom) potential energy increase during the melting of crystalline zircon. Cooling of the zircon melt under zero applied pressure to room temperature leads to an amorphous state with equilibrium density according to the current potential model of zircon. The above amorphous state (HD) has higher internal energy and has about 11% volume swelling as compared to crystalline zircon. The simulated glass has a glass transition temperature at about 2000 K as indicated by the change of slope in both the cooling curves of the energy and volume versus temperature.

TABLE IV. Comparison of the experimental and simulated structure and properties of alpha-quartz ($P3_221$) using the potential model of this work.

	Simulation	Experiment[a]
a (Å)	4.943	4.916
c (Å)	5.450	5.405
Volume/SiO_2 (Å^3)	38.46	37.71
Si (u)	0.4693	0.4697
O (x)	0.4293	0.4135
O (y)	0.2648	0.2669
O (z)	0.7971	0.7857
Si-O	1.587/1.594	1.614/1.605
O-Si-O	110.6/115.0	109.0/110.5
	108.1/108.1	108.8/109.2
Si-O-Si	150.9	143.7
B_o (GPa)	37	38

[a] Reference 44.

TABLE V. Comparison of the experimental and simulated structure of tetragonal zirconia ($P4_2/NMC$) using the potential model of this work.

	Simulation	Experiment[a]
a (Å)	3.597	3.605
c (Å)	5.086	5.179
c/a	1.414	1.437
Volume/ZrO_2 (Å^3)	32.9	33.7
d_z[b]	0.062	0.065
Zr-O	2.202/2.202	2.102/2.351
B_o (GPa)	228	

[a] References 45 and 46.

[b] d_Z is the relative displacement of oxygen atoms in alternating columns in the Z direction.

The calculated neutron structure factors and neutron broadened total correlation functions are shown in Fig. 2 for the LD and HD glasses. The neutron structure factors were calculated by adding the partial structure factors multiplied by the weighting factors determined by composition and neutron scattering length,[34,35]

$$S_N(Q) = \left(\sum_{i=1}^{n} c_i b_i\right)^{-2} \sum_{i,j=1}^{n} c_i c_j b_i b_j S_{ij}(Q), \tag{3}$$

where c_i is the mole fraction of atoms, b_i is the neutron scattering length, for species i. $S_{ij}(Q)$ is the partial structure factor of the atom pair i and j, which can be calculated through Fourier transformation of the pair distribution functions (PDF),

$$S_{ij}(Q) = 1 + \rho_o \int_0^R 4\pi r^2 [g_{ij}(r) - 1] \frac{\sin(Qr)}{Qr} \frac{\sin(\pi r/R)}{\pi r/R} dr, \tag{4}$$

where $g_{ij}(r)$ is the pair distribution function of atom pair i and j, Q is the scattering vector, ρ_o is the average atom number density, and R is the maximum value of the integration in real space which is set to half of the size of one side of the simulation cell. The $[\sin(\pi r/R)]/(\pi r/R)$ part is a Lortch type window function to reduce the effect due to the finite cutoff of r.

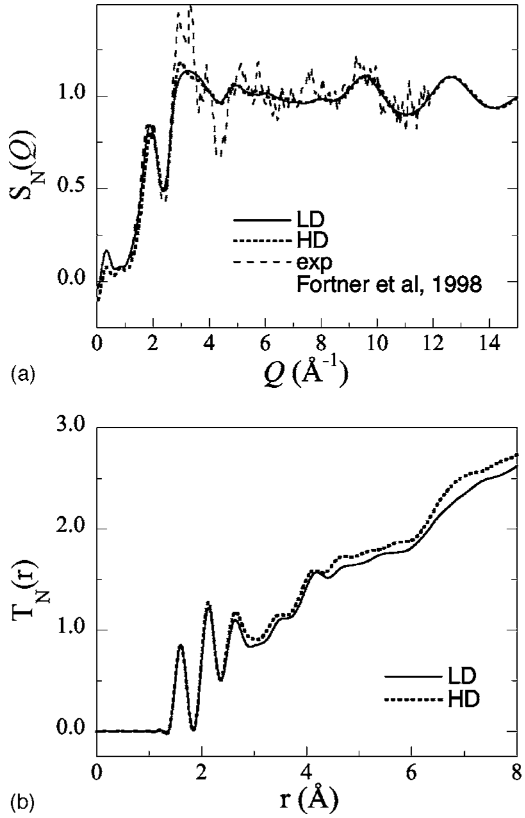

FIG. 2. (a) Neutron structure factors of HD (dotted) and LD (solid) amorphous zircon compared with the experimental data from Fortner, Badyal, Price, Hanchar, and Weber.[20] (b) Neutron broadened total correlation functions of HD and LD amorphous zircon.

The neutron structure factors [Fig. 2(a)] are similar for the LD and HD amorphous states with minor differences on the first two peaks. The LD state has a slightly stronger first peak and is located at a lower Q value (at 1.88 Å^{-1} for LD and 1.95 Å^{-1} for HD) than the HD amorphous state. The second peak of the HD has a peak at around 3.5 Å^{-1} and a shoulder at around 4.0 Å^{-1}, while the LD state only has a broad peak at around 3.8 Å^{-1}. The features beyond 8 Å^{-1} are almost identical for both HD and LD amorphous states. The high Q part of the structure factor correlates with short range structure features, while the features at low Q and the first peak in particular (normally named first sharp diffraction peak FSDP)[34] are related to the medium range structure of amorphous materials. The similarity of the structure factors at high Q of the LD and HD amorphous states of zircon suggest that their local environments around zirconium and silicon are very similar. Differences in the features of the FSDP and other low Q features manifest the differences in the medium range structure that manifests between the LD and HD amorphous states. This is supported by the neutron broadened total correlation functions [Fig. 2(b)]. The first two peaks, corresponding to the Si-O and Zr-O distributions respectively, are almost identical for the LD and HD states. The third peak that comprises contributions of the first peaks of Zr-Zr, Zr-Si, Si-Si, and O-O pair distributions peaks shows considerable differences of the two states.

Figure 2 also compares the structure factors of the simulated amorphous zircon with the experimental data from neutron diffraction study of completely amorphous zircon.[20] The experimental zircon sample was doped with ^{238}Pu and accumulated three times the dose necessary to fully amorphize zircon.[20] The authors have attributed the noise in the experimental data to the limited sample size demanded by restrictions associated with the Pu contents. In addition, the residual features at 2.91 Å^{-1} and 3.32 Å^{-1} in the experimental structure factor were suggested to be due to the vanadium container used during the measurement or possibly quartz crystal due to minor phase separation. In view of the above,

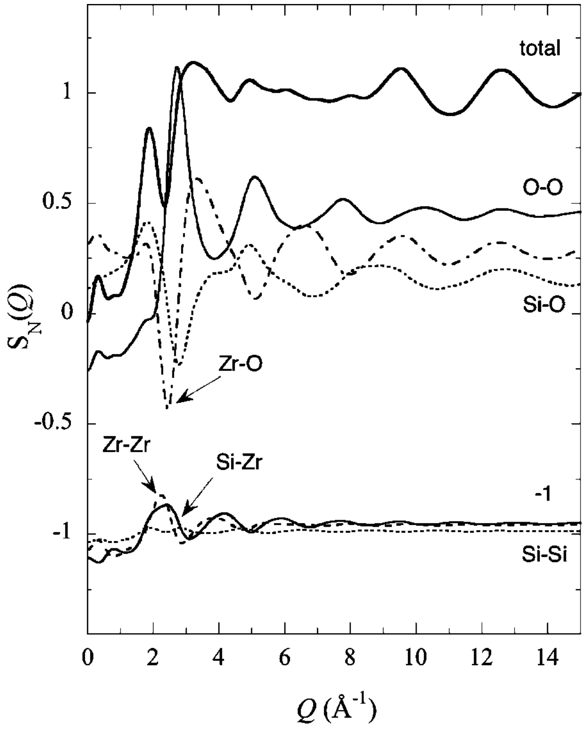

FIG. 3. Partial neutron structure factors of the LD glass.

the agreement between simulation and the experimental neutron structure factor is reasonable. In particular, the position and intensity of the first diffraction peak from simulation show excellent agreement with experiments. Except for the above-mentioned features at around 3 Å^{-1}, the experimental data oscillates around the structure factors from simulation, suggesting that the amorphous zircon from the simulation is a good representation of the experimental amorphous zircon structure. However, new experimental work on neutron diffraction of amorphous zircon with improved data quality will be highly desirable for better comparison between simulation and experiment.

The total neutron structure factor was decomposed into partial structure factors to obtain information of the contributions of the atom pairs to the total structure factor (shown in Fig. 3). The first sharp diffraction peak (FSDP) in network amorphous systems has been shown to have correlations to the medium range structure.[36,37] The decomposition can help to understand the experimental structure factors, especially the contributions to the FSDP, where the partial structure factor can not be readily obtained experimentally. The major contributions to the FSDP are from the Si-Zr, Zr-Zr pairs and Zr-O and Si-O pairs. Both the polymerization of the Si-O network and clustering of Zr-O regions can contribute to the medium range structure. Contributions to the fairly broad second peak are from the O-O first peak and the second Zr-O and Si-O peak. The difference of the FSDP in the HD and LD amorphous zircon manifests slight differences of their medium range structure.

Figure 4 shows the Si-O (a) and Zr-O (b) PDFs for LD, HD amorphous zircon, as well as the crystalline zircon, at 300 K. The first peaks of the Si-O PDF from HD and LD amorphous zircon are very well defined but slightly broadened and shifted to larger Si-O distances compared to the crystal form. The coordination number of silicon (shown in Table VI) is also found to be around 4, suggesting that the silicon-oxygen tetrahedral structure is maintained. In the non-balanced partial-charge model used in a previous MD study of amorphous zircon, the silicon coordination number was found to be 3.5.[25] The two peaks associated with the two sets of Zr-O distances in crystalline zircon evolve into a single peak in the amorphous states. The first Zr-O peak shifts from the 2.13 Å in crystalline zircon to 2.10 Å in the amorphous forms. The Zr-O coordination numbers range from five to nine with the average coordination number of 6.46 for LD and 6.61 for HD (Table VI). The results are in agreement with the EXAFS studies of metamict zircon.[14] The Zr-O distance was found to decrease by 0.06 Å and average Zr coordination number decreased to 6.8–7.2±0.5.[14] Both the bond length shortening and reduction of coordination number are observed in the simulated amorphous zircon

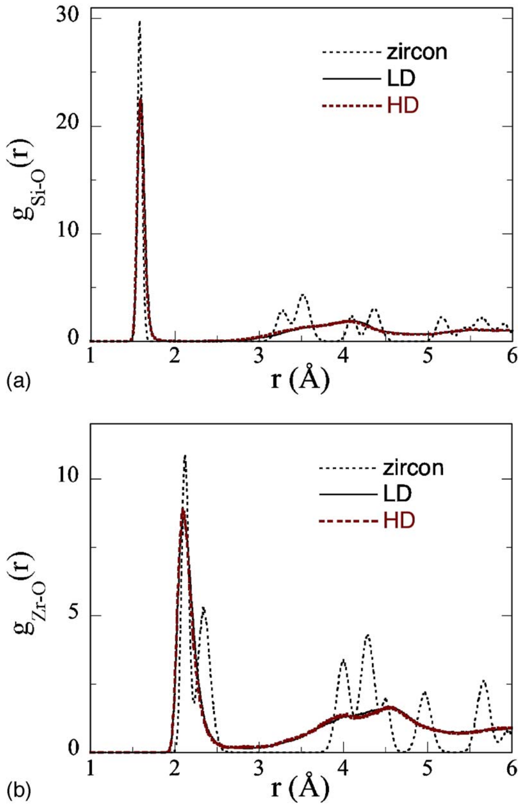

FIG. 4. (Color online) Si-O (a) and Zr-O (b) pair distribution functions of crystalline zircon (solid line), LD (dotted line) and HD (dashed line) amorphous zircon.

TABLE VI. Average cation coordination numbers.[a]

Glass	Silicon	Zirconium
LD	4.11	6.46
LD-big	4.02	6.44
HD	4.04	6.61

[a] Coordination numbers are calculated using a Si-O cutoff distance of 2.2 Å and a Zr-O cutoff distance of 3.0 Å.

TABLE VII. Comparison of bond length and bond angle of amorphous and crystalline zircon.

	Zircon-crystal	HD	LD
Bond length (Å)			
Si-O	1.62	1.59	1.60
Zr-O	2.13/2.27	2.10	2.10
Si-Zr	2.99/3.63	3.40	3.48
Zr-Zr	3.61	3.41/3.85	3.42/3.85
Si-Si	3.61	3.10	3.13
O-O		2.59	2.59
Bond angle (degree)			
O-Si-O	97/116	107	108
Si-O-Si	—	146	145
Si-O-Zr	111/150	95/125	98/127
O-Zr-O	60-150	78	80
Zr-O-Zr	111	102	102

structures. The bond length and bond angles of simulated amorphous zircon and zircon crystal are summarized in Table VII.

As shown in Fig. 4, the crystal features of the Si-O and Zr-O PDFs at longer distances disappear in LD and HD amorphous zircon indicating the loss of long range order. Other PDFs shown later have similar trend.

Figure 5 shows the cation-cation PDFs that have important information of how the cation oxygen polyhedra are connected. The first Si-Si peaks of the LD and HD amorphous zircon [Fig. 5(a)] shift to 3.13 and 3.10 Å, respectively, from 3.61 Å in crystalline zircon. The rather dramatic change of the Si-Si PDF first peak position indicates the existence of corner sharing SiO_4 in amorphous zircon; while in the crystal form, all the SiO_4 tetrahedra are isolated. The polymerization of SiO_4 tetrahedra has been observed in metamict zircon by Si NMR studies.[17] The Si-O-Si bond angle distribution and Q^n distribution, shown later, further quantify the polymerization of the SiO_4 tetrahedra.

The Si-Zr PDFs are shown in Fig. 5(b). Two Si-Zr distances exist in crystalline zircon: 2.99 Å for edge-sharing SiO_4 and ZrO_8 polyhedrons and 3.63 Å for corner-sharing ones. In the amorphous forms, the peak due to edge-sharing is greatly depressed and becomes a shoulder; while the peak due to corner-sharing is broadened and shifts to a slightly shorter distances of around 3.4 Å. X-ray diffraction studies found that the first Si-Zr peak in the crystal form disappeared in the amorphous form, which was explained by the loss of edge-sharing SiO_4 and ZrO_8 polyhedrons, consistent with observations in simulated amorphous zircon.[15]

The Zr-Zr PDFs are shown in Fig. 5(c). In amorphous zircon, the Zr-Zr peak splits into two peaks, one at around 3.4 Å and one at around 3.9 Å, shorter and longer than the 3.61 Å of Zr-Zr first peak in the crystal form, respectively. In the zircon crystal, all the ZrO_8 dodecahedrons are edge-shared; while in the amorphous forms, zirconium oxygen polyhedrons differentiate into two groups, edge- and face-sharing ZrO_x polyhedrons contributing to the first Zr-Zr peak and corner-sharing polyhedrons to the second peak. The shortening of the Zr-Zr distance in edge-sharing ZrO_x polyhedrons can be explained by the decrease of Zr coordination number from 8 in the crystal to a value of 6–7 in amorphous form and a corresponding shortening of Zr-O distances [shown in Fig. 4(b)]. A considerable amount (shown later) of face-sharing of ZrO_x polyhedra were observed, which contribute to the shorter Zr-Zr distances. The second Zr-Zr peak is due to corner-sharing ZrO_x polyhedrons that do not exist in zircon crystal. Figure 6(a) shows a snapshot of corner and edge-sharing ZrO_x polyhedra in amorphous zircon. In Fig. 6(b), the connectivities of the cation polyhedra in crystalline zircon are shown: edge- and corner sharing of SiO_4 and ZrO_8 and edge-sharing of ZrO_8 dodecahedra. The change of Zr-Zr distance is in good agreement with EXAFS and diffraction studies.[13–15] EXAFS studies observed a shortened Zr-Zr dis-

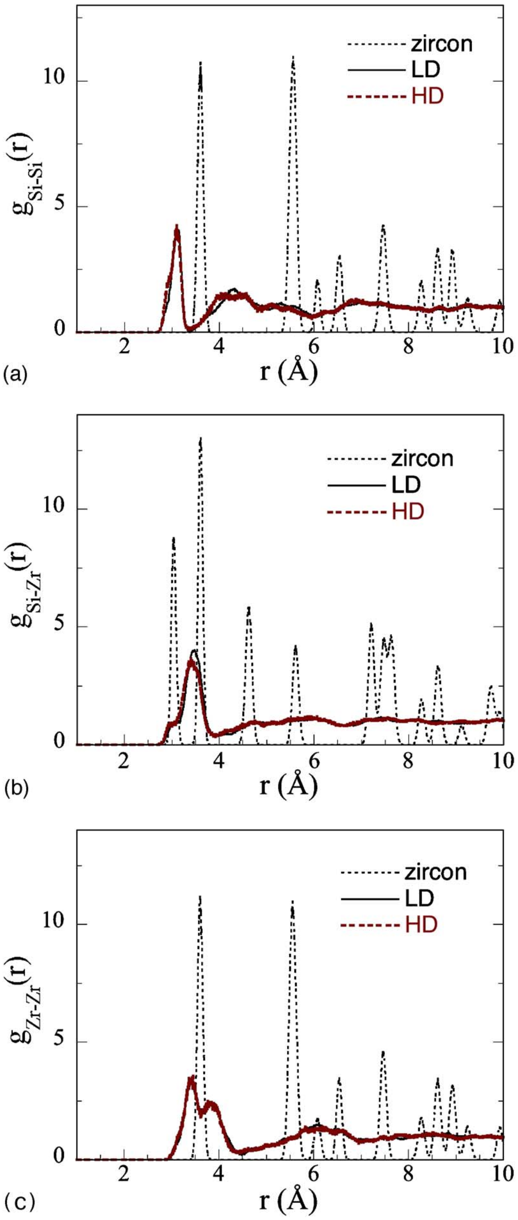

FIG. 5. (Color online) Cation-cation pair distributions of crystalline zircon (solid line), LD (dotted line) and HD (dashed line) amorphous zircon (a) Si-Si, (b) Si-Zr, (c) Zr-Zr.

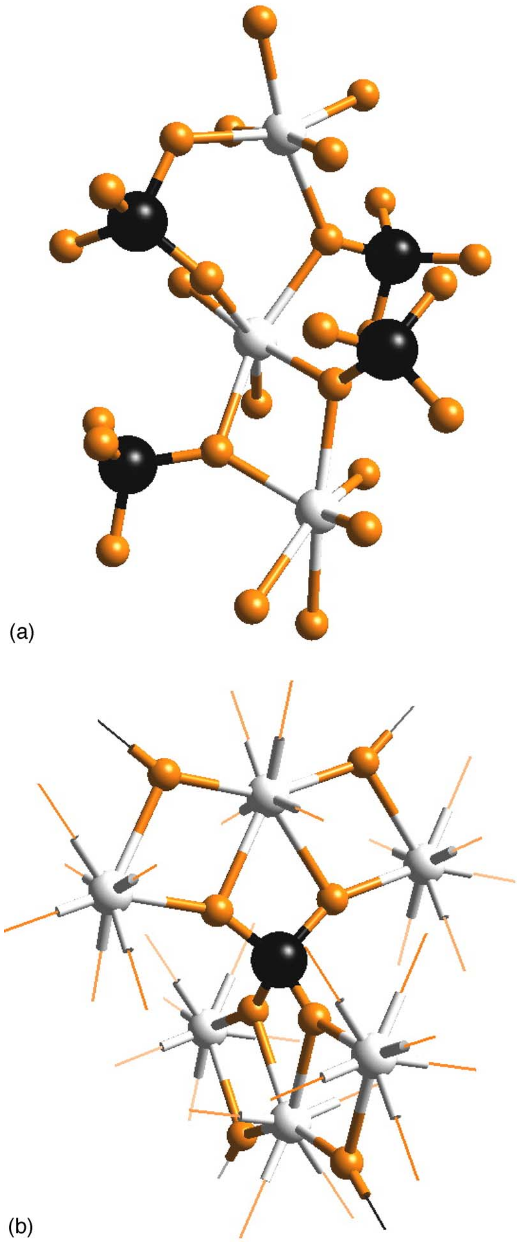

FIG. 6. (Color online) (a) Snapshots showing corner- and edge-sharing zirconium oxygen polyhedra in simulated zircon glass (LD). (b) Cation oxygen polyhedra connection in zircon crystal. Black ball: silicon, small dark gray ball: oxygen, large light gray ball: zirconium.

tance of 3.3–3.4 Å in metamict natural zircon.[14] Another EXAFS study observed two sets of Zr-Zr distances in the amorphous form of Pu doped zircon.[15]

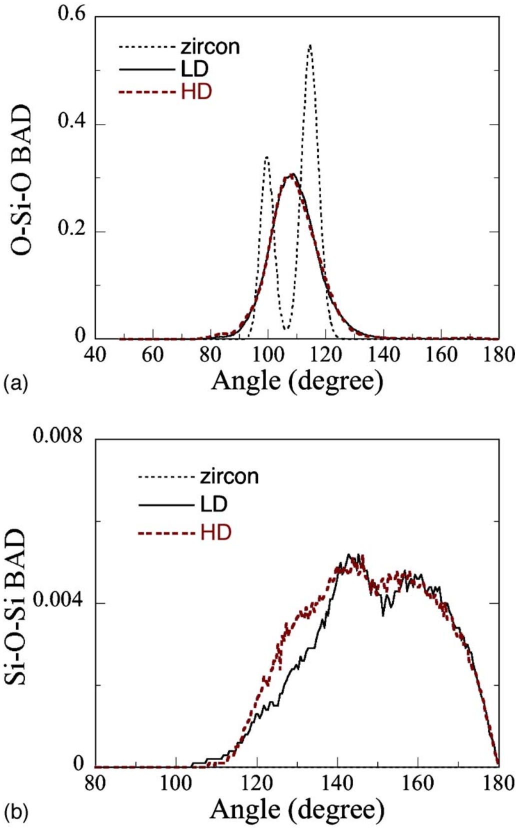

FIG. 7. (Color online) O-Si-O (a) and Si-O-Si (b) bond angle distributions of cation-cation pair distributions of crystalline zircon (dotted line), LD (solid line), and HD (dashed line) amorphous zircon.

Figure 7 shows O-Si-O [Fig. 7(a)] and Si-O-Si [Fig. 7(b)] bond angle distributions. Two characteristic O-Si-O bond angles exist in crystal zircon: one around 97 and one around 116 degrees, respectively. The difference of the two O-Si-O bond angles is due to edge-sharing of SiO_4 with ZrO_8 polyhedra that leads to an elongation of the SiO_4 tetrahedra along the c-axis. In the amorphous forms, the SiO_4 tetrahedra tend to be more symmetric with a single peak at around 108 degrees, close to the ideal tetrahedral angle of 109.47 degrees. The Si-O-Si bond angle distributions of both the HD and LD amorphous phases show a major peak at around 145 degrees and a minor peak at around 155 degrees. The presence of Si-O-Si bond angle distributions reveals the polymerization of the SiO_4 tetrahedra. In comparison, there is no Si-O-Si linkage in crystalline zircon where all the SiO_4 tetrahedra are isolated.

Further characterization of the amorphous zircon structure was performed by determining the statistics of the Q^n distributions and the distribution of oxygen species (shown in Table VIII). Q^n, meaning n bridging oxygen per SiO_4 tetrahedron, distributions are obtained from silicon NMR studies and have been used to analyze the network connectivity of silicate minerals and glasses.[16,17,38] The Q^n species in the simulated amorphous zircon range in n value from 0 to 4, consistent with recent NMR studies of metamict zircon.[16] The existence of higher Q^n species $(n \geqslant 1)$ confirms the polymerization of the SiO_4 tetrahedra. The average Q^n for LD and HD are 1.66 and 1.81, respectively, suggesting an increase of n and indicating greater SiO_4 polymerization in higher density amorphous states. The Q^n values of the amorphous zircon in this work are consistent with the value of 1.5 from a recent *ab initio* molecular dynamics simulations of LD amorphous zircon[19] and those from NMR studies[16] with the correction of the empirical scale to interpret the experimental data.[19] A previous MD simulation reported average Q^n value of 1.95 for the LD amorphous zircon.[25]

TABLE VIII. Distributions of Q^n species in the simulated amorphous zircon.

		Q^n species (%)					Oxygen species (%)		
Glasses	Ave. Q^n	Q^0	Q^1	Q^2	Q^3	Q^4	FO	NBO	BO
LD	1.66	15.0	28.9	34.2	19.2	2.7	20.4	58.9	20.6
LD-big	1.78	10.2	30.3	35.9	18.4	5.1	21.8	55.9	22.3
HD	1.81	10.6	31.8	30.8	23.4	4.3	21.6	55.9	22.5

The distributions of oxygen species are also shown in Table VIII. The oxygen species were determined by the number of silicon coordination around each oxygen ion: an oxygen ion is considered to be a free oxygen (FO) if no silicon ion is within its first coordination shell; similarly, nonbridging oxygen (NBO) and bridging oxygen (BO) are oxygen ions with one and two silicon in its first coordination shell, respectively. For instance, all oxygen ions are BO in quartz and ideal silica glass but NBO in crystalline zircon. All three species of oxygen exist in amorphous zircon, with the FO and BO each around 20% and NBO around 60%. Since the FO is only bonded by zirconium ions, the rather high FO percentage is indicative of regions rich in zirconium. Similarly, the high percentage of BO together with the existence of Q^3 and Q^4 species indicates that there exist silicon rich regions. A fragment of connected SiO_4 tetrahedra that forms a chain is shown in Fig. 8. The percentages of FO and BO increase, while that of NBO decreases, in the HD compared to the LD amorphous form.

The cation environments around oxygen ions (as shown in Table IX) in the zircon system provide an indicator of the change in nearest neighbor structure and configurational entropy of the melt and the glass as compared to the crystalline state. In crystalline zircon, there exists only one type of oxygen environment 1Si2Zr (meaning one silicon and two zirconium in the first coordination shell of oxygen). In the melt, there is a dramatic decrease of the 1Si2Zr coordination combination to 22.4%, while there is an increase of all other cation coordination combinations that range from 2 to 4 cations around oxygen. The 1Si1Zr is the largest at 31.3% followed by 2Si at 12.4% and 3Zr at 12.1%. Among all the amorphous states (LD, LD-big, and HD), the cation coordinations around oxygen are similar and remained distributed amongst different cation combinations as in the melt. A considerable increase of the 1Si2Zr combination to 31–33% and a decrease of 1Si1Zr to 21–25% are observed as compared to the melt. The dramatic increase of the complexity of the cation environments around oxygen ions from the crystalline state to the melt and the amorphous states suggests an large increase of configurational entropy, which indicates the fragility of the zircon melt[39] and thus partly explains the difficulty to form a glass state from the zircon melt.

To further characterize the medium range structure, we obtained the statistics of the size of the polymerized Si-O network. Tables X–XII show the statistics of the size of the polymerized Si-O network fragments in LD, HD, and LD-big, respectively. Except for 10–15% of the total SiO_4 tetrahedrons being isolated, most of the SiO_4 are polymerized to some degree. The largest SiO_4 network fragment size depends on the simulation size, ranging from around 130 for LD and HD to around 1100 for LD-big. The fraction of the total tetrahedrons in the largest fragment, however, remains around 50% in all three cell sizes. The result that over half of the SiO_4 tetrahedrons are polymerized indicates that there are possible energetic reasons behind the polymerization. We also performed similar calculations on the ZrO_x polyhedra size distribution and found that all the ZrO_x polyhedra are connected in all the amorphous structures studied. The percolation of the ZrO_x network is not surprising since in the crystalline zircon structure, all the ZrO_8 dodecahedrons are connected. The difference between the percolated zirconium oxygen network in the amorphous and crystalline zircon lies in the fact that the zirconium oxygen polyhedra are connected through corner, edge and face-sharing in the amorphous form, while they are connected only through face-sharing in the crystal.

The statistics of the primitive ring size distribution was also performed and the results are shown in Fig. 9. The HD

TABLE IX. Cation environments around oxygen in crystalline, melt, and amorphous zircon.[a]

	Percentage of cation combinations								
	2Si	1Si1Zr	2Zr	1Si2Zr	2Si1Zr	3Zr	1Si3Zr	4Zr	Others
Zircon Melt (4800 K)	12.4	31.3	8.5	22.6	6.9	12.1	2.3	1.4	2.5
LD	15.9	24.8	2.6	32.3	4.4	14.9	1.9	3.0	0.2
LD-big	17.2	23.7	2.4	30.9	5.0	16.0	1.2	3.4	0.2
HD	17.1	20.6	1.9	32.9	5.1	16.9	2.6	2.8	1.1

[a] Coordination numbers are calculated using a Si-O cutoff distance of 2.2 Å and a Zr-O cutoff distance of 3.0 Å.

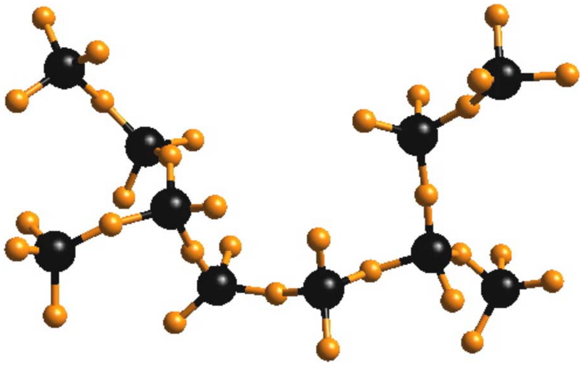

FIG. 8. (Color online) Fragments of connected silicon-oxygen tetrahedra (zirconium atoms removed) in simulated zircon glass (LD) showing Q^1, Q^2, and Q^3 species. Black ball: silicon, small gray ball: oxygen.

amorphous zircon has a higher concentration of rings with sizes from 1-12, but less rings with size larger than 12. This is consistent with the fragment size distribution where there are more isolated SiO_4 tetrahedrons in LD than the HD amorphous structure. The LD-big has considerably larger rings (35–40) than the LD and HD, which can be explained by that larger simulation cell allows larger ring to form. In general, the number of rings per base Si (with maximum 0.15) in amorphous zircon is much lower than that of silica with a value of around 3.5. Although there exist considerable polymerization of the Si-O network and large fragments of silicon-oxygen network in amorphous zircon most of the fragments are in the shape of chains or branched chains, only a small fractions of the Si-O network form rings.

DISCUSSION

Amorphization of zircon by radiation damage due to the decay of the actinide constituents is known to dramatically change the chemical durability of zircon where it was found that the dissolution rate of amorphous zircon is 1–2 orders of magnitudes higher than the crystalline form.[40,41] Characterization of the amorphous structure provides a structural basis to understand these dramatic changes in the pure amorphous phase, thereby providing a contrast to the crystal phase. The considerable volume swelling accompanying the amorphization opens the structure and enhances the cation diffusion and hydration. The decrease of the zirconium coordination number from 8 in the crystal to 6–7 in the glass also weaken the chemical bond that can enhance the dissolution process at the amorphous surface and crystal/amorphous interfaces.[42] Our simulation results show that the amorphous zircon structure is characterized by the polymerization of the silicon-oxygen tetrahedra and formation of regions rich in zirconium. This kind of micro-segregation provides diffusion channels of zirconium ions and could ease the dissolution of fragments of silicon-oxygen networks that together increase the dissolution rate of amorphous zircon.

Crystalline zircon is a type of orthosilicate in which all the SiO_4 tetrahedra are isolated by other cation oxygen poly-

TABLE X. Si-O network fragment size statistics of LD.

Fragment size # of Si	Number of fragments	Si atom percentage
1	38	14.8
2	4	3.1
3	5	5.7
4	1	1.6
5	1	2.0
10	1	3.9
17	1	6.6
31	1	12.1
128	1	50.0

TABLE XI. Si-O network fragment size statistics of HD.

Fragment size # of Si	Number of fragments	Si atom percentage
1	28	10.9
2	7	5.5
3	5	5.9
4	1	1.6
5	2	3.9
6	1	2.3
7	1	2.7
40	1	15.6
132	1	51.6

TABLE XII. Si-O network fragment size statistics of LD-big.

Fragment size # of Si	Number of fragments	Si atom percentage
1	209	10.2
2	64	6.3
3	24	3.5
4	11	12.2
5	5	31.2
6	6	1.8
7	4	1.4
8	3	1.2
9	1	0.4
10	1	0.5
16	3	2.3
18	1	0.9
19	1	0.9
23	2	2.3
28	1	1.4
32	2	3.1
66	1	3.2
76	1	3.7
1098	1	53.6

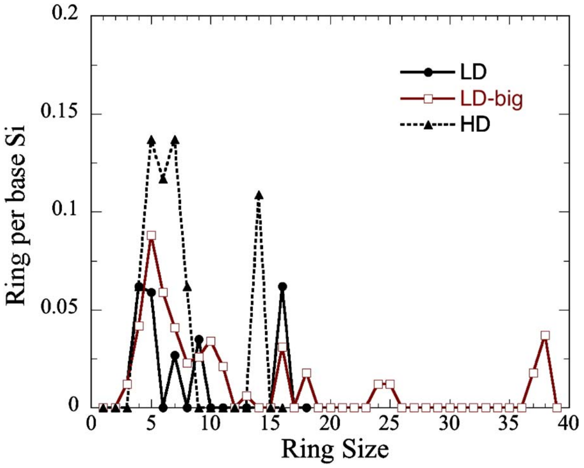

FIG. 9. (Color online) Primitive ring statistics of the polymerized Si-O network.

hedrons. Amorphization leads to the polymerization of SiO_4 tetrahedra and the formation of fragments of silicon-oxygen networks in zircon in agreement with ^{29}Si NMR studies.[16,17] The n value from Q^n statistics in simulated amorphous zircon is 1.6-1.8, suggesting that the polymerization is lower than that to form a fully linear chain structure of SiO_4 polyhedrons. In common crystalline silicates, a SiO_4 chain structure is formed when n equals 2, a layered structure is formed when n equals 3 and a three dimensional network is formed when n is 4. Examining the distribution of Q^n (Table VIII) species show that there exist a wide range of n values ranging from 0 to 4 suggesting that there exist isolated SiO_4 tetrahedra and highly polymerized regions. Most of the networks are found to be chain-like as shown in Fig. 8. In crystalline zircon, each oxygen is bonded to three cations, two zirconium and one silicon ion, whereas the polymerization creates bridging oxygen sites (BO, each oxygen bond to only two silicon). The amorphous structures respond to the polymerization of silicon oxygen tetrahedra by generating a small fraction (around 5%) of higher coordinated oxygen ions, such as four zirconium or one silicon and three zirconium ions, while lowering the zirconium coordination number from 8 in crystalline zircon to 6-7 in amorphous zircon. It is worth noting that, although the zirconium coordination number decreases, the silicon coordination number remains around four after polymerization. The latter occurs because the higher field strength of the smaller silicon ion favors maintaining an optimal coordination number of four oxygen ions around silicon.

Another way to consider the polymerization effect is by the average number of oxygen ions per SiO_4. In crystalline zircon, since all the oxygen ions are non-bridging oxygen, there are four oxygen ions per SiO_4. In the polymerized structure of amorphous zircon, the average Q^n is around 1.8, which means that average number of oxygen ions per SiO_4 is 3.1-3.2 since each bridging oxygen ion is shared by two silicon ions. The difference leads to about 20% oxygen ions that are not connected to any silicon ion, i.e., free oxygen (FO), which is consistent with the statistics of oxygen species in amorphous zircon shown in Table VIII. A recent *ab initio* MD simulation found that the average n value of Q_n species is around 1.5.[19] In the NMR study of fully metamict zircon, the average n value of Q^n species was found to be around 3.[16] It was shown later that the empirical scale used to obtain the average n value from experiment was incorrect, and a value close to 1.5 was obtained when corrections was made on this scale.[19]

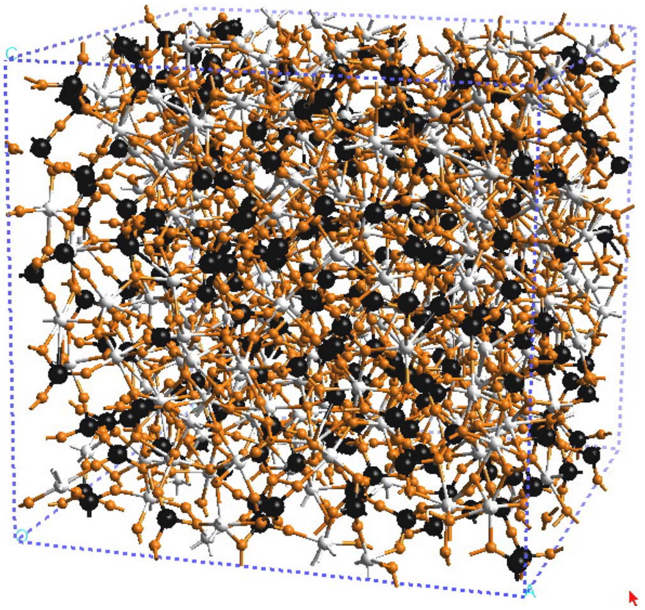

FIG. 10. (Color online) Snapshot of simulated amorphous zircon structure (LD, 4×4×4, 1536 atoms). Black ball: silicon, small dark gray ball: oxygen, large light gray ball: zirconium.

The wide distribution of Q_n species, high percentage of free oxygen, and the existence of oxygen ions that are solely bonded to silicon or zirconium ions together indicate that there exist atomic-scale regions rich in silicon-oxygen network (shown in Fig. 8) and regions rich in zirconium (shown in Fig. 11). The silicon rich regions and zirconium rich regions are intermingled together as can be seen in Fig. 10 and Fig. 11. During the annealing of the amorphous zircon, the silicon rich regions can be precursors to form amorphous or crystalline silica while the zirconium rich regions can nucleate to form crystalline zirconia. It has been observed in x-ray diffraction[43] and EXAFS[14] studies of step annealing of amorphous zircon that some amorphous silica and monoclinic zirconia may begin to form at intermediate temperatures before fully recrystallizing into crystalline zircon at high temperature. Long-term annealing of the amorphous zircon state directly to intermediate temperatures can lead to phase separation into amorphous silica and monoclinic zirconia.[15] In the simulated amorphous zircon structure, the zirconium coordination number of around 7 and the existence of OZr_3 and OZr_4 coordinations are similar to the cation and anion environment in monoclinic zirconia, which agrees well with the experimental observations.

The sample size effect on the melting and amorphous zircon structure has been studied. A $4\times4\times4$ zircon super cell with 1536 atoms and a $6\times6\times6$ zircon super cell with 5184 atoms were used in the study of the melting process of zir

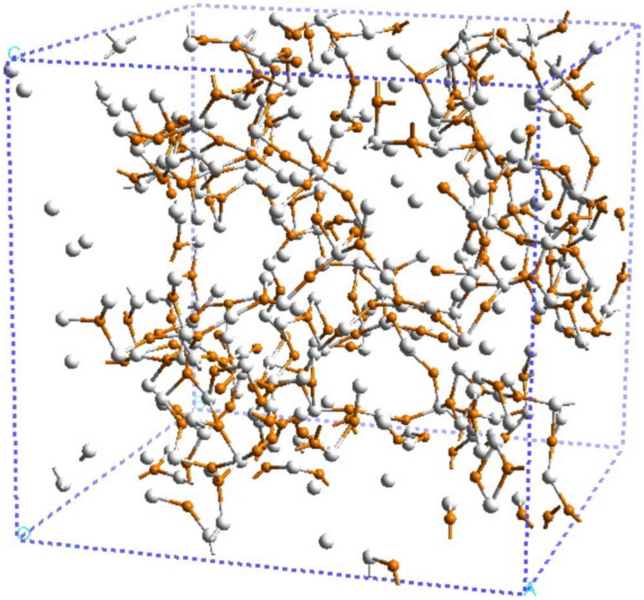

FIG. 11. (Color online) Snapshot of simulated amorphous zircon structure (LD, 4×4×4, 1536 atoms) with all the silicon and coordinated oxygen ions removed and only zirconium atoms and free oxygen ions left. Small dark gray ball: oxygen, large light gray ball: zirconium.

con. In both cases, the zircon crystal melted at about 4800 K, and the volume expansion and internal energy change accompanying the melting process were also very similar. This reveals that the simulation cell size effect is minimal. The quenching (under constant pressure) of the melted zircon of the two sample sizes generated amorphous phases with similar volume expansion (around 11%) relative to crystalline zircon, which is slightly lower than the volume change observed experimentally (around 18%).[1]

Two amorphous zircon samples, LD and LD-big corresponding to amorphous phases with 18% volume expansion, were compared. The LD and LD-big have 1536 and 12288 atoms in the simulation cells and correspond to 4×4×4 and 8×8×8 zircon super cells, respectively. Although the general structure features of LD and LD-big amorphous zircon are very similar, there are observable differences on the statistics of Q^n, distributions of oxygen species and bond angle distributions. The average n value of Q^n species is 1.66 for LD, lower than that of 1.78 for LD-big. The percentage of BO and FO are 20.4 and 20.6 for LD, and 21.8 and 22.3 for LD-big, respectively. The differences of the Si-O-Si bond angle distributions for the LD and LD-big amorphous zircon are shown in Fig. 12. The higher BO and FO percentage, together with higher average n of Q^n species, in the LD-big amorphous zircon than those in LD seemed to suggest that a larger simulation cell slightly favors higher polymerization of the silicon-oxygen network and the formation of larger zirconium-FO segregated regions. However, it is possible that some of the differences between LD and LD-big is purely statistical where averaging over independently generated LD samples can lead to better agreement between LD and LD-big structures.

Experimentally, it is found that volume swelling of fully amorphized zircon is around 18%.[1] The simulation of low density (LD) and high density (HD), corresponding to 18% and 11% volume swelling, respectively, make it possible to compare the structure differences for these two amorphous structures. The LD and HD amorphous zircon have in general very similar structure. The HD phase has slightly shorter bond length (Table VII and Figs. 4 and 5) and higher zirconium coordination number (Table VI). The HD phase also has higher average n values of Q^n species and higher percentage of BO and FO. The HD phase seemed to have slightly more polymerized silicon-oxygen network and more clustered regions of zirconium, which is consistent with experimental annealing data that suggests some polymerization of silica and clustering of zirconia during early stages of recovery of the volume expansion.[43] These results show that the Teter potential is well suited to model not only the structure and properties of crystalline zircon and end member oxides but also the short and medium range structure of amorphous zircon.

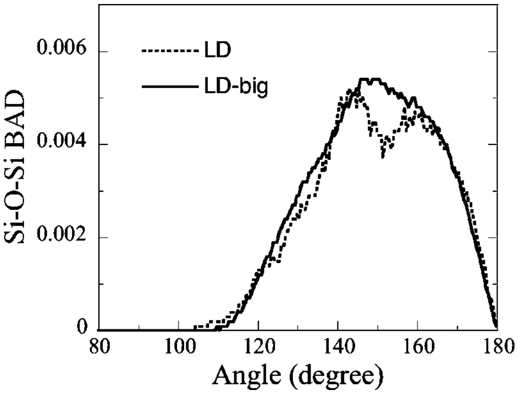

FIG. 12. Si-O-Si bond angle distributions in LD and LD-big amorphous zircon.

CONCLUSIONS

Molecular dynamics simulations were used to study the structure of amorphous zircon by employing a charge balanced partial-charge pair-wise potential capable of describing the structure and properties of crystalline zircon and end member oxides. The amorphous zircon structure is characterized by polymerization of the SiO_4 tetrahedra that form branched chains like structures, which intermingle together with regions rich in zirconium. The medium range structures of amorphous zircon were characterized by the fist sharp diffraction peak (FSDP), silicon-oxygen network fragment size and primitive ring size distributions. It is found that only about 10–15% of the silicon oxygen tetrahedra are isolated while the rest of them are polymerized to some degree to form mostly branched chains and rings with different sizes. The zirconium-oxygen network was found to percolate with zirconium oxygen polyhedra connected via corner, edger or face-sharing. This contrasts the connected zirconium oxygen dodecahedra, all via edge-sharing, in the crystal form.

In amorphous zircon, the silicon ions maintain their oxygen coordination number of four while the SiO_4 tetrahedra are more symmetric than those in the zircon crystal. Zr-O distances are shorter than those in the crystalline form and the average Zr coordination number decreases to 6–7 in amorphous zircon. These structural changes lead to stabilizing the amorphous phase. The average n of the Q^n species is 1.6–1.8 and there is a considerable percentage of (20%) free oxygen ions bonded only to zirconium indicating the existence of silicon and zirconium rich regions in the amorphous zircon structure. The decrease of the Zr coordination number and the resulting decrease of cation coordination number around O weaken the chemical bonds. These structural changes coupled with the observed micro-segregation that introduce interfacial structures can lead to increase of ion diffusion and dissolution in amorphous zircon.

ACKNOWLEDGMENTS

This research is supported by the Divisions of Materials Sciences and Engineering and Chemical Science, Office of Basic Energy Sciences, U.S. Department of Energy. This research was performed in part using the Molecular Science Computing Facility in the William R. Wiley Environmental Molecular Sciences Laboratory (EMSL) at the Pacific Northwest National Laboratory (PNNL). The EMSL is funded by DOE's Office of Biological and Environmental Research. Battelle operates PNNL for DOE.

---

*Current address: Department of Chemical Engineering, University of Virginia, Charlottesville, VA 22904. Electronic address: jd9xc@virginia.edu

†Current address: Departments of Materials Science and Engineering, and of Chemistry, The University of Arizona, Tucson, AZ 85721.

[1] W. J. Weber, R. C. Ewing, and L. M. Wang, J. Mater. Res. **9**, 688 (1994).

[2] R. C. Ewing, W. Lutze, and W. J. Weber, J. Mater. Res. **10**, 243 (1995).

[3] G. M. Rignanese, F. Detraux, X. Gonze, A. Bongiorno, and A. Pasquarello, Phys. Rev. Lett. **89**, 117601 (2002).

[4] E. Balan, D. R. Neuville, P. Trocellier, E. Fritsch, J.-P. Muller, and G. Calas, Am. Mineral. **86**, 1025 (2001).

[5] A. Meldrum, L. A. Boatner, and R. C. Ewing, Phys. Rev. B **56**, 13805 (1997).

[6] L. Bbsail, N. Hamelin, and P. D. Towsend, Nucl. Instrum. Methods Phys. Res. B **59/60**, 1219 (1991).

[7] M. A. Russak, C. V. Jahnes, and E. P. Katz, J. Vac. Sci. Technol. A **7**, 1248 (1989).

[8] G. D. Wilk and R. M. Wallace, Appl. Phys. Lett. **76**, 112 (2000).

[9] W.-J. Qi, R. Nieh, E. Dharmarajan, B. H. Lee, Y. Jeon, L. Kang, K. Onishi, and J. C. Lee, Appl. Phys. Lett. **77**, 1704 (2000).

[10] S. Ellsworth, A. Navrotsky, and R. C. Ewing, Phys. Chem. Miner. **21**, 146 (1994).

[11] M. Nogami, J. Non-Cryst. Solids **69**, 415 (1985).

[12] R. C. Ewing, A. Meldrum, L. M. Wang, W. J. Weber, and L. R. Corrales, in *Zircon* (Mineralogical Society of America, Washington, 2003), Vol. 53, p. 387.

[13] F. Farges and G. Calas, Am. Mineral. **76**, 60 (1991).

[14] F. Farges, Phys. Chem. Miner. **20**, 504 (1994).

[15] B. D. Begg, N. J. Hess, W. J. Weber, S. D. Conradson, M. J. Schweiger, and R. C. Ewing, J. Nucl. Mater. **278**, 212 (2000).

[16] I. Farnan and E. K. H. Saije, J. Appl. Phys. **89**, 2084 (2001).

[17] I. Farnan, H. Cho, W. J. Weber, R. D. Scheele, N. R. Johnson, and A. E. Kozelisky, Rev. Sci. Instrum. **75**, 5232 (2004).

[18] I. Farnan, Phase Transitions **69**, 47 (1999).

[19] E. Balan, F. Mauri, C. J. Pickard, I. Farnan, and G. Calas, Am. Mineral. **88**, 1769 (2003).

[20] J. A. Fortner, Y. Badyal, D. C. L. Price, J. M. Hanchar, and W. J. Weber, in *Materials Research Society Symposium Proceedings*, edited by S. J. Zinkle, G. E. Laucas, R. C. Ewing, and J. S. Williams (Materials Research Society, Warrendale, PA, 1999), Vol. 540, p. 349.

[21] P. J. Wasilewski, F. E. Senftle, J. E. Vaz, A. N. Thorpe, and C. C. Alexander, Radiat. Eff. **17**, 191 (1973).

[22] M. Zhang, E. K. H. Salje, I. Farnan, A. Graeme-Barber, P. Daniel, R. C. Ewing, A. M. Clark, and H. Leroux, J. Phys. Condens. Matter **12**, 1915 (2000).

[23] M. Zhang and E. K. H. Salje, J. Phys. Condens. Matter **13**, 3057 (2001).

[24] M. Zhang, E. K. H. Salje, G. C. Capitani, H. Leroux, A. M. Clark, J. Schluter, and R. C. Ewing, J. Phys. Condens. Matter **12**, 3131 (2000).

[25] R. Devanathan, L. R. Corrales, W. J. Weber, A. Chartier, and C. Meis, Phys. Rev. B **69**, 064115 (2004).

[26] D. M. Teter (private communication).

[27] J. F. Ziegler, J. P. Biersack, and U. Littmark, *The Stopping Power and Range of Ions in Matter* (Pergamon, New York, 1985).

[28] W. Smith and T. R. Forester, J. Mol. Graphics **14**, 136 (1996).

[29] R. M. Hazen and L. W. Finger, Am. Mineral. **64**, 196 (1979).

[30] H. Ozkan, L. Cartz, and J. C. Jamieson, J. Appl. Phys. **45**, 556 (1974).

[31] J. P. Crocombette and D. Ghaleb, J. Nucl. Mater. **257**, 282 (1998).

[32] J. M. Delaye and D. Ghaleb, J. Nucl. Mater. **244**, 22 (1997).

[33] B. Park, W. J. Weber, and L. R. Corrales, Phys. Rev. B **64**, 174108 (2001).

[34] J. Du and L. R. Corrales, Phys. Rev. B **72**, 092201 (2005).

[35] J. Du and L. R. Corrales, J. Non-Cryst. Solids **352**, 3255 (2006).

[36] S. R. Elliott, Nature **354**, 445 (1991).

[37] S. R. Elliott, Phys. Rev. Lett. **67**, 711 (1991).

[38] J. F. Stebbins, J. Non-Cryst. Solids **106**, 359 (1988).

[39] C. A. Angell, J. Phys. Chem. Solids **49**, 863 (1988).

[40] R. C. Ewing, D. J. Haachar, and W. Lutze, in *Scientific Basis for Nuclear Waste Management V*, edited by W. Lutze (Materials Research Society, Pittsburgh, PA, 1982), p. 389.

[41] R. C. Ewing, Proc. Natl. Acad. Sci. U.S.A. **96**, 3432 (1999).

[42] E. Balan, F. Mauri, D. A. Muller, and G. Calas, Am. Mineral. **86**, 910 (2001).

[43] W. J. Weber, Radiat. Eff. Defects Solids **115**, 341 (1991).

[44] L. Levien, C. T. Prewitt, and D. J. Weidner, Am. Mineral. **65**, 920 (1980).

[45] C. J. Howard, R. Hill, and B. E. Reichert, Acta Crystallogr. **44**, 116 (1988).

[46] G. Teufer, Acta Crystallogr. **15**, 1187 (1962).